

## Article

# Improvement of X-ray Photoelectric Conversion Performance of MAPbI<sub>3</sub> Perovskite Crystals by Ionic Liquid Treatment

Xueqiong Su <sup>\*</sup>, Ruimin Wang , Huimin Yu, Jin Wang, Ruixiang Chen, He Ma and Li Wang <sup>\*</sup>

School of Physics and Optoelectronic Engineering, Beijing University of Technology, Beijing 100124, China; loriawang@emails.bjut.edu.cn (R.W.); yhm\_holly@163.com (H.Y.); wangjinbjut321@163.com (J.W.); chenruixiang@emails.bjut.edu.cn (R.C.); mahe\_beijing@bjut.edu.cn (H.M.)

<sup>\*</sup> Correspondence: nysxq@bjut.edu.cn (X.S.); lwang.1@bjut.edu.cn (L.W.)

**Abstract:** Although perovskite has great potential in optoelectronic devices, the simultaneous satisfaction of material stability and high performance is still an issue that needs to be solved. Most perovskite optoelectronic devices use quantum dot spin coating or the gas-phase growth of perovskite thin films as the photoelectric conversion layer. Due to stability limitations, these materials often experience a significant decrease in photoelectric conversion efficiency when encountering liquid reagents. The self-assembled growth of hybrid perovskite crystals determines superior lattice ordering and stability. There are three types of ionic liquids—[Emim]BF<sub>4</sub>, EMIMNTF<sub>2</sub>, and HMITFSI—that can effectively enhance the X-ray photoelectric conversion performance of hybrid perovskite crystal CH<sub>3</sub>NH<sub>3</sub>PbI<sub>3</sub> (MAPbI<sub>3</sub>), and the enhancement in the photocurrent leads to an improvement in the sensitivity of X-ray detectors. We soak the perovskite crystals in an ionic liquid and perform two treatment methods: electrification and dilution with ETOH solution. It is interesting to find that MAPbI<sub>3</sub> perovskite single crystal materials choose the same optimized ionic liquid species in X-ray detection and photovoltaic power generation applications, and the effect is quite the opposite. Compared with untreated MAPbI<sub>3</sub> crystals, the average photocurrent density of Electrify-HMITFSI MAPbI<sub>3</sub> increased by 826.85% under X-ray excitation and the sensitivity of X-ray detectors made from these treated MAPbI<sub>3</sub> crystals significantly increased by 72.6%, but the intensity of the PL spectrum decreased to 90% of the untreated intensity.

**Keywords:** perovskite; MAPbI<sub>3</sub> crystals; ionic liquid treated; X-ray photoelectric conversion; X-ray detector



**Citation:** Su, X.; Wang, R.; Yu, H.; Wang, J.; Chen, R.; Ma, H.; Wang, L. Improvement of X-ray Photoelectric Conversion Performance of MAPbI<sub>3</sub> Perovskite Crystals by Ionic Liquid Treatment. *Coatings* **2024**, *14*, 633. <https://doi.org/10.3390/coatings14050633>

Academic Editors: Alessandro Latini and Sangmo Kim

Received: 21 April 2024

Revised: 6 May 2024

Accepted: 13 May 2024

Published: 16 May 2024



**Copyright:** © 2024 by the authors. Licensee MDPI, Basel, Switzerland. This article is an open access article distributed under the terms and conditions of the Creative Commons Attribution (CC BY) license (<https://creativecommons.org/licenses/by/4.0/>).

## 1. Introduction

Perovskite demonstrates a remarkable photoelectric conversion efficiency and optical absorption coefficient, endowing it with a broad spectrum of applications in solar cells, photodetectors, and various optoelectronic devices [1]. Halide perovskite single crystals have more advantages compared to other perovskite materials, such as a stronger light absorption, better carrier transport properties, and greater stability [2].

The basic chemical formula of the perovskite crystal is ABX<sub>3</sub> [3]. The CH<sub>3</sub>NH<sub>3</sub>PbI<sub>3</sub> (MAPbI<sub>3</sub>) crystal is a typical organic–inorganic hybrid perovskite crystals. In comparison to other MAPbX<sub>3</sub> perovskites, the presence of iodine at the x position in the MAPbX<sub>3</sub> crystal results in a higher atomic number and a narrower band gap, rendering it more suitable for application as an X-ray detector among perovskite crystals [4]. Sergii Yakunin et al. demonstrated the potential of MAPbI<sub>3</sub> for medical X-ray detection by achieving a near-100% external quantum efficiency and fast response speed in photoconductive and optoelectronic devices, comparable to traditional X-ray detection equipment of the time [5]. However, MAPbX<sub>3</sub> crystals are less stable in air, which makes the development of X-ray detectors based on MAPbX<sub>3</sub> slower than others. To fully capitalize on the potential of this material, the performance improvements in MAPbX<sub>3</sub> crystals have focused on surface defect passivation [6]. Using ionic liquids offers a promising avenue for further improvement.

Ionic liquids are liquids composed entirely of anions and cations that remain in a liquid state at or near room temperature, representing a new generation of environmentally friendly electrolyte materials that have found widespread application in the field of optoelectronics. Due to their high electron density, ionic liquids have the capability to occupy halogen defects induced by halogen ion migration in perovskite [7].

There are two methods for using ionic liquids to treat perovskite materials, which are commonly used in the field of solar cells. Firstly, ionic liquids can be added as additives into the perovskite precursor solution to improve the crystallization quality of perovskite films by interacting with the perovskite. Secondly, the surface of perovskite films can be coated with ionic liquids. The utilization of ionic liquids for passivating perovskite surface defects can substantially improve the performance of perovskite photovoltaic devices. Li et al. used [Bmim]BF<sub>4</sub> to modify and protect perovskite solar cells, achieving a PCE of 19.30%. This indicates that the [Bmim]BF<sub>4</sub> coating can protect the perovskite layer from degradation due to water and oxygen exposure, thereby enhancing device stability [8]. Zhang et al. found that [Emim]BF<sub>4</sub> ionic liquid reduces surface and grain boundary defects in perovskite, leading to secondary grain growth and smaller grain size [9].

The selection of ionic liquids is diverse. Common cations include those found in pyridinium, imidazolium, and quaternary ammonium, while prevalent anions consist of halides (X<sup>-</sup>), formates (HCOO<sup>-</sup>), and tetrafluoroborate (BF<sub>4</sub><sup>-</sup>) [7]. Different ionic liquids exert varying effects on perovskite performance. Zhao et al. treated MAPbI<sub>3</sub> thin films with three ionic liquids and found that HMITFSI treatment led to a 6% increase in photoelectric conversion efficiency [10]. In 2023, Su et al. treated MAPbI<sub>3</sub> crystals with [Emim]BF<sub>4</sub> and EMIMNTF2 ionic liquids, respectively, observing an enhancement in the optical properties of MAPbI<sub>3</sub> crystals treated with both ionic liquids [11].

Although ionic liquids have been shown to significantly enhance the optical and electrical properties of perovskites, research on their application to improve the photoelectric conversion performance of MAPbI<sub>3</sub> crystals under X-ray excitation is still limited. Therefore, we employed [Emim]BF<sub>4</sub>, EMIMNTF2, and HMITFSI to fabricate MAPbI<sub>3</sub> crystals using either electric immersion or mixed ETOH immersion methods. We evaluated the optical and photoelectric conversion properties of the MAPbI<sub>3</sub> crystals both before and after immersion, compared the treated MAPbI<sub>3</sub> crystals, and examined the influence of the aforementioned three ionic liquids and two treatment methods on the properties of MAPbI<sub>3</sub> X-ray detectors. Based on the experimental data, we preliminarily inferred the formation mechanism of these outcomes. This study provides a reference value for improving the perovskite X-ray detector sensitivity.

## 2. Experiment

### 2.1. Materials

Lead (II) iodide (99.99%) (PbI<sub>2</sub>) was procured from Aladdin, while Methylammonium iodide (99.5%) (MAI) was sourced from Macklin (Shanghai, China). Additionally,  $\gamma$ -Butyrolactone (99%) was purchased from MREDA (Beijing, China), and the rigid interdigital electrode was obtained from Guangzhou Mecart Sensor Technology (Guangzhou, China). Furthermore, 1-Hexyl-3-methylimidazole bis(trifluoromethyl) sulfonimide salt (HMITFSI) was acquired from Monils Chem. Eng. Sci. & Tech. (Shanghai) Co., Ltd. (Shanghai, China). The compounds 1-Ethyl-3-methylimidazolium tetrafluoroborate ([Emim]BF<sub>4</sub>) and 1-Ethyl-3-methylimidazole bis(trifluoromethyl) sulfonimide salt (EMIMNTF2) were obtained from Shanghai Aichun Biological Technology Co., Ltd. (Shanghai, China). All other materials were sourced from Beijing University of Technology (Beijing, China).

### 2.2. Crystallization

Crystallization was achieved using the inverse temperature method. The steps are as follows: 461 mg of PbI<sub>2</sub> is mixed with 156 mg of MAI at room temperature and dissolved in 1 mL of  $\gamma$ -butyrolactone. The solution is then transferred into a heating mantle, stirred with a magnetic rotor at 60 °C for 30 min until fully dissolved, and subsequently removed.

The heated solution is filtered through a 25 mm PTFE filter. To facilitate the growth of large crystals, seed crystals composed of small MAPbI<sub>3</sub> are introduced into the filtered liquid. The filtered liquid is then placed in a heating mantle and reheated at a rate of 2 degrees Celsius per minute until it reaches 100 degrees Celsius. By maintaining the supersaturated precursor solution at 100 °C for three hours, stable, high-quality, large crystals can be produced. Experimental photographs are depicted in Figure S1 of the Supporting Information.

### 2.3. Ionic Liquid Treatment Process

When the ionic liquid acts as a surface modifier, we can study the effects of these three ionic liquids on the surface defects of the MAPbI<sub>3</sub> perovskite crystals without altering their structure.

The self-assembled growing MAPbI<sub>3</sub> was separately immersed in 2 mL of different ionic liquids. We linked the ionic liquid to the 1.5V battery with a copper wire. We allowed the MAPbI<sub>3</sub> to soak in the solution of electricity for approximately 10 min to ensure uniform contact between the perovskite crystals and the ionic liquid. After soaking, we air-dried the perovskite crystals at room temperature for approximately 2 h. The crystals produced via this method are designated as Electrify-[Emim]BF<sub>4</sub> MAPbI<sub>3</sub>, Electrify-EMIMNTF<sub>2</sub> MAPbI<sub>3</sub>, and Electrify-HMITFSI MAPbI<sub>3</sub>.

In another treatment approach, we dissolved 3 μL of the respective ionic liquid in 5 mL of ETOH. Once fully dissolved, we carefully immersed the MAPbI<sub>3</sub> crystal in the liquid for soaking, which should last for 10 min. We ensured the perovskite surface was completely submerged in the mixture. Following soaking, we allowed the perovskite crystals to fully dry at room temperature for 2 h. The crystals produced using this method are denoted as ETOH-[Emim]BF<sub>4</sub> MAPbI<sub>3</sub>, ETOH-EMIMNTF<sub>2</sub> MAPbI<sub>3</sub>, and ETOH-HMITFSI MAPbI<sub>3</sub> (Figure 1).

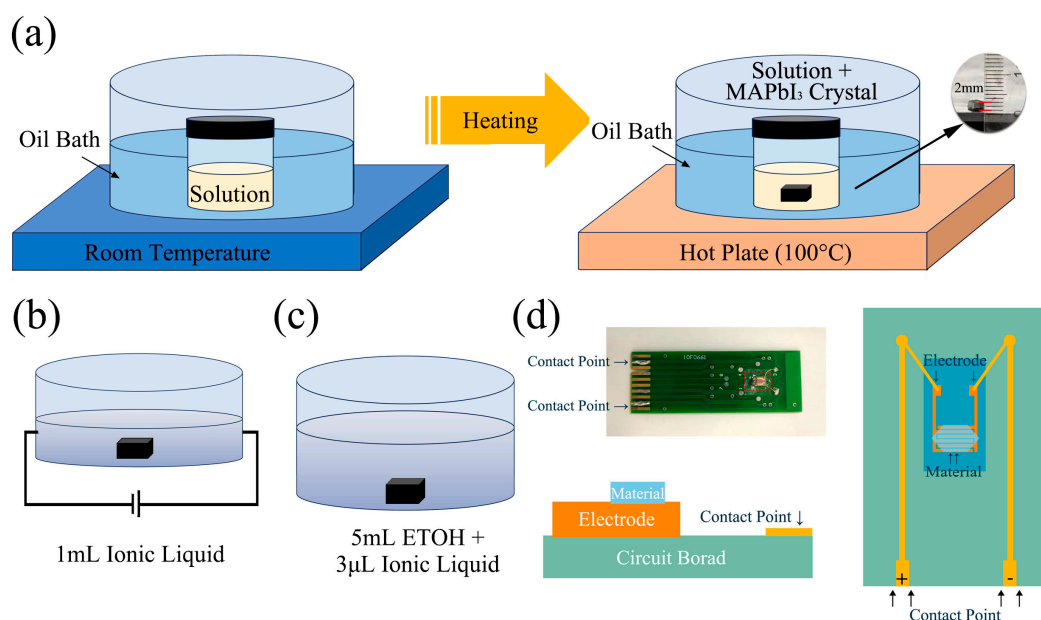


**Figure 1.** (a) Preparation of MAPbI<sub>3</sub> crystal; (b) Preparation of electrify-ionic liquid MAPbI<sub>3</sub>; (c) Preparation of ETOH-ionic liquid MAPbI<sub>3</sub>; (d) The structure of the prepared X-ray detector.

### 2.4. Device Fabrication of X-ray Detector

To assemble the X-ray detector, the crystal was affixed to an interdigital electrode using conductive silver adhesive. The electrode, depicted in Figure S2 of the Supporting Information, measures 4 mm in width and 6 mm in length, with a linewidth of 5 μm, comprising a total of 25 pairs of fingers. Following testing, both ends of the electrode

remain open under both illuminated and non-illuminated conditions, with no current generated in the circuit.

The MAPbI<sub>3</sub> crystal was positioned on the electrode and secured in place using conductive silver glue. Using a multimeter, the resistance of the treated portion of the crystal (approximately in the kilohms range) can be measured at both ends, ensuring proper circuitry.

### 2.5. Characterization

The microstructure of perovskite crystals was analyzed using X-ray diffraction (XRD) with a Bruker D8 Advanced instrument. The morphology of the perovskite crystals was observed through scanning electron microscopy (SEM) using a JEOL JSM 6500F microscope. The charge distribution and energy-level structure were determined via X-ray photoelectron spectroscopy (XPS) using an Escalab 250XI instrument. Photoluminescence (PL) spectra were obtained using the spectrometers NIR512 and S2000. Electrical performance was measured using a DC regulated power supply (Keysight B2902). The X-ray source was provided by the Bruker D8 Discover instrument. All experiments were conducted at standard room temperature.

## 3. Results and Discussion

### 3.1. Structure and Surface Morphology of MAPbI<sub>3</sub> Crystal

The analysis of untreated MAPbI<sub>3</sub> samples was conducted using an XRD instrument, as depicted in Figure 2a. The ionic-treated crystals were cut and XRD tested on the interior and surface. The results reveal a well-oriented crystal plane in the untreated MAPbI<sub>3</sub> crystal and interior after treatment, with all peaks indexed as the perovskite tetragonal phase. However, the crystal surface presents the orthogonal crystal phase after the ionic liquid treatment, indicating that the ionic liquid treatment changes the crystal structure of the material surface. The absorption spectrum reveals that the band gap of MAPbI<sub>3</sub> is approximately 1.56 eV, corresponding to broadband absorption at a wavelength of less than 800 nm, as shown in Figure 2b. It means that the untreated MAPbI<sub>3</sub> perovskite crystals are of a good quality [12].

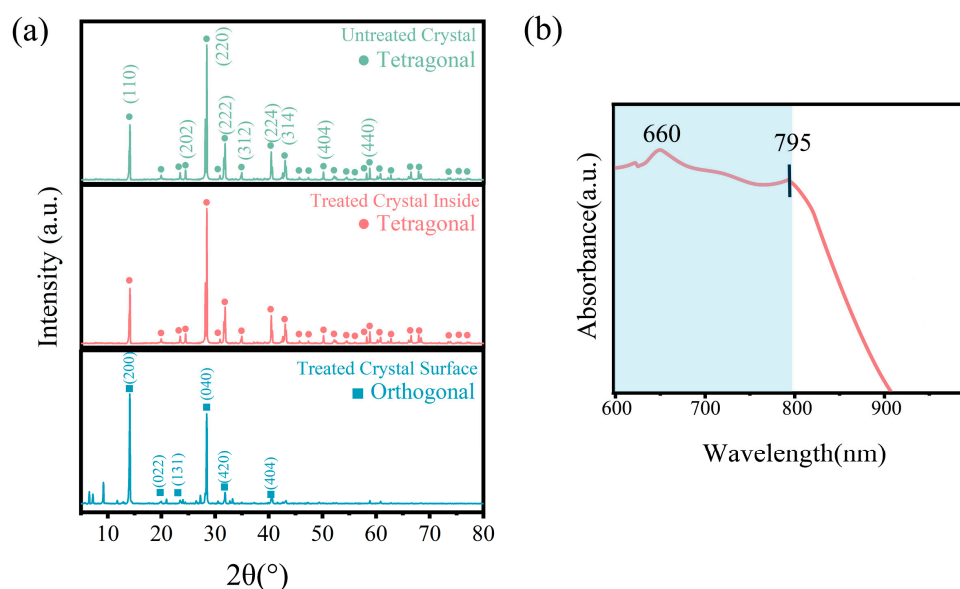


**Figure 2.** (a) XRD patterns of MAPbI<sub>3</sub> crystals; (b) Absorption spectrum of untreated MAPbI<sub>3</sub> crystals.

The SEM images of the surface of MAPbI<sub>3</sub> crystals treated with ETOH mixed ionic liquids are shown in Figure 3. For alcohol-based organic compounds, experiments have shown that the miscibility range between ionic liquids and alcohol mixed systems gradually

increases with the increasing length of the alkyl side chains of the ionic liquids. Therefore, ionic liquids with shorter alkyl side chains can be miscible with alcohol systems, as for the three ionic liquids used in this study.

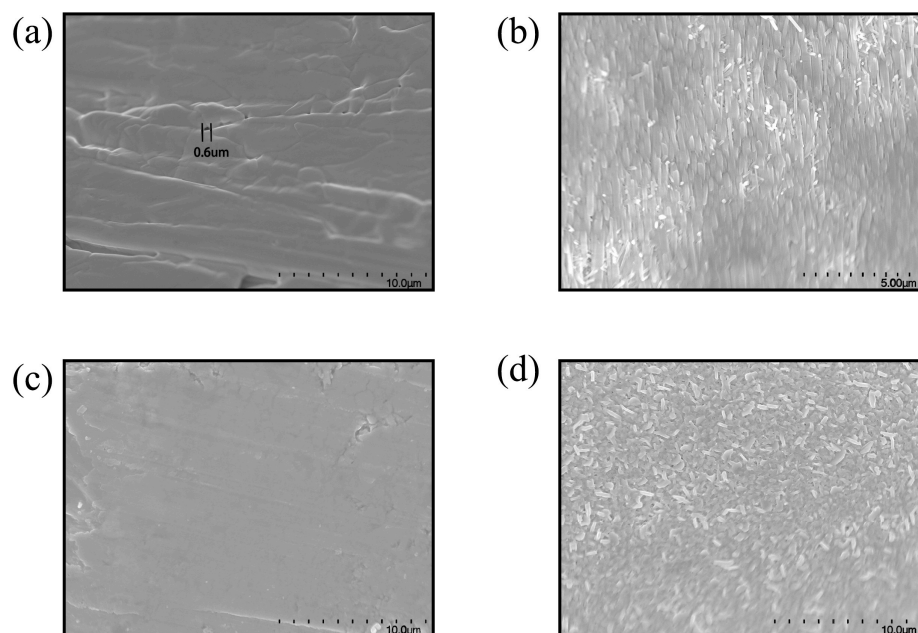


**Figure 3.** SEM of MAPbI<sub>3</sub>: (a) original MAPbI<sub>3</sub>; (b) [Emim]BF<sub>4</sub> MAPbI<sub>3</sub>; (c) EMIMNTF2 MAPbI<sub>3</sub>; (d) HMITFSI MAPbI<sub>3</sub>.

Compared to untreated MAPbI<sub>3</sub>, immersion in EMIMNTF2 ionic liquids resulted in the formation of a nearly membranous coating on the surface of the MAPbI<sub>3</sub>, making the originally rough surface smoother. The surfaces of [Emim]BF<sub>4</sub> MAPbI<sub>3</sub> and HMITFSI MAPbI<sub>3</sub> perovskite crystals experience disintegration and show a squamous structure. The squamous structure surface will form obvious grain boundaries and dislocations, while increasing the surface area. The scales on the scaly surface of HMITFSI MAPbI<sub>3</sub> crystal were smaller in size and even showed signs of shedding.

It has been reported that in the mixed system achieved after mixing with ETOH, the hydrogen bonding interactions between ETOH molecules are continuously strengthened. As a result, the self-diffusion coefficients of the ions in the system increase, and the viscosity of the system decreases while the conductivity increases. The increase in conductivity of the mixed system indicates an enhancement in the electrical properties of the ionic liquid [13].

For the EMIMNTF2 MAPbI<sub>3</sub> crystal, the existing surface defects of the MAPbI<sub>3</sub> were improved, and the electronic environment was optimized compared to before. For the [Emim]BF<sub>4</sub> MAPbI<sub>3</sub> and HMITFSI MAPbI<sub>3</sub> perovskite crystals, the interactions occurring on the surface also triggered a small number of crystal phase transitions, as shown in XRD patterns.

Figure 4 shows SEM images of the cross-sections of the MAPbI<sub>3</sub> before and after treatment, demonstrating a change in the cross-sectional state of the treated crystal compared to the untreated one. As seen in Figure 4a, the untreated MAPbI<sub>3</sub> interface appears bamboo-like, which is the result of the layered self-growth of the MAPbI<sub>3</sub>. After HMITFSI electrify treatment, the MAPbI<sub>3</sub> interface structure as it shows in Figure 4b, tends to a rock-like texture, indicating a change in phase transition after exciton recombination, making the MAPbI<sub>3</sub> crystal structure closer to a single crystal. On the other hand, in Figure 4c, the cross-section of MAPbI<sub>3</sub> soaked in ETOH-[Emim]BF<sub>4</sub> displays a significant discontinuity. The layer thickness resulting from soaking is 70 μm, and a distinct crystal boundary is visible beneath this layer.

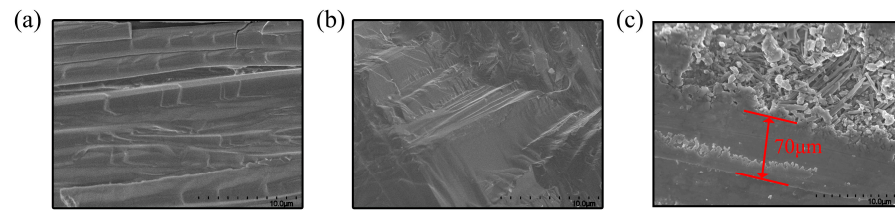


**Figure 4.** Cross-section of MAPbI<sub>3</sub>. (a) untreated; (b) After ionic liquid electrify treatment; (c) after ETOH mixed ionic liquid treatment.

### 3.2. Optical Properties of MAPbI<sub>3</sub> Crystal

The photoluminescence (PL) spectra of MAPbI<sub>3</sub> crystals before and after treatment with ionic liquids were observed by irradiating them with a 355 nm laser, as shown in Figure 5. The PL peaks come from the direct electron transition radiation in the MAPbI<sub>3</sub> crystal. The Electrify-EMIMNTF2 MAPbI<sub>3</sub> crystal photoluminescence properties exhibited the most significant increase in peak intensity. The peak intensity increased by approximately 200%, with the PL peak wavelength shifting from 773 nm to 769 nm, exhibiting a slight blue shift. The Electrify-[Emim]BF<sub>4</sub> MAPbI<sub>3</sub> crystal did not exhibit a blue shift, with the emission peak located at 773 nm, and the peak intensity increased by approximately 100%. For the Electrify-HMITFSI MAPbI<sub>3</sub> crystal, the emission peak showed a blue shift, located at 770 nm, while the light intensity decreased to about 90% of the original sample. The peak positions of the changes in peak intensity reflect the efficiency of charge carrier separation. In simple terms, the higher the peak, the faster the rate of carrier recombination, while a lower peak indicates an easier separation of photo-induced charges. Comparing the peak intensities, it can be observed that Electrify-HMITFSI MAPbI<sub>3</sub> is the sample with the easiest separation of photo-induced charges, while Electrify-EMIMNTF2 MAPbI<sub>3</sub> exhibits the highest rate of carrier recombination.

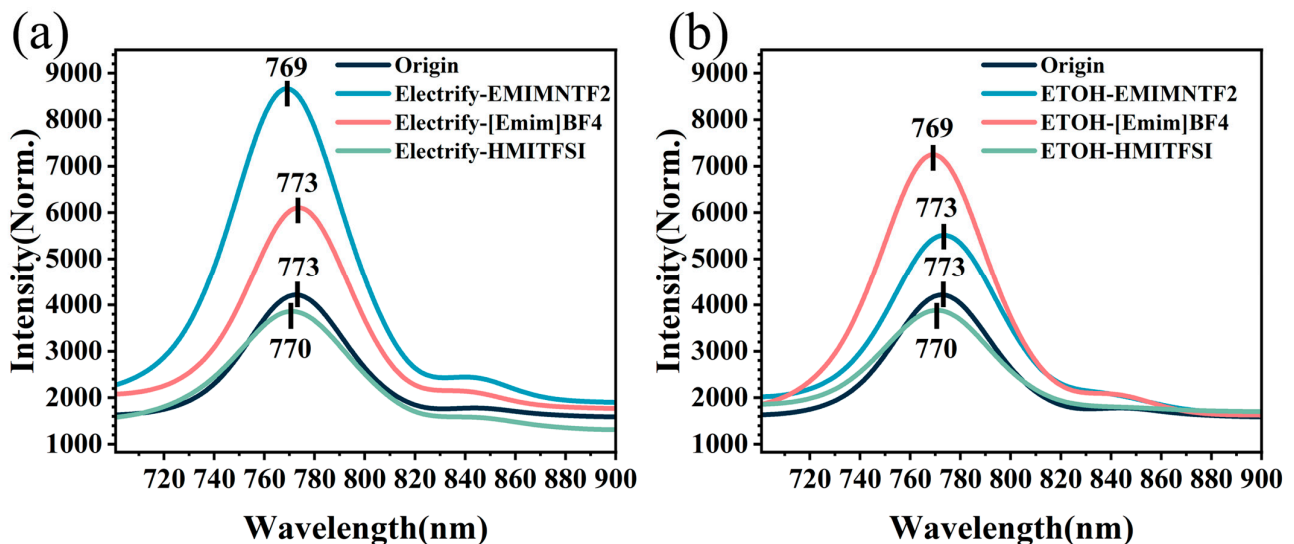


**Figure 5.** PL spectrum of MAPbI<sub>3</sub> crystals: (a) after electric immersion in ionic liquids; (b) after immersion in ionic liquid mixed with ETOH.

The other dilution with ETOH solution treatment method is consistent with the change law of the photoluminescence characteristics obtained by the electrification method. Compared to the electrify-treated crystals, the type of ionic liquid and treatment methods have a decisive effect on the photoluminescence characteristics of perovskite crystals, and the effect of electrification treatment is better. ETOH-[Emim]BF<sub>4</sub> MAPbI<sub>3</sub> resembles the luminescent properties of the Electrify-EMIMNTF2 MAPbI<sub>3</sub> crystal. The peak intensity increased by approximately 200%, with the wavelength shifting from 773 nm to 769 nm, exhibiting a

slight blue shift. ETOH-EMIMNTF2 MAPbI<sub>3</sub> resembles the Electrify-[Emim]BF<sub>4</sub> MAPbI<sub>3</sub> crystal and the peak intensity increased by approximately 50%. In terms of peak intensity, both [Emim]BF<sub>4</sub> and EMIMNTF2 ionic liquids, under two different treatment methods, enhanced the light intensity at the peak position of the MAPbI<sub>3</sub> crystals, resulting in an increased rate of carrier recombination. For HMITFSI, neither of the two different treatment methods resulted in an increase in light intensity for the treated MAPbI<sub>3</sub>; instead, a decrease was observed, making the separation of photo-induced charges more easily achievable.

For perovskite materials, the migration of positively charged iodide vacancies or neutral iodide Frenkel defects towards the negative electrode can lead to a decrease in PL intensity. Particularly for MAPbI<sub>3</sub> films used in solar cells, the films between the electrodes typically contain a certain density of positively charged iodide vacancies and a larger density of negative iodide gaps, which are often considered as P-type doping. When a voltage is applied across the electrodes, the positively charged iodide vacancies drift towards the negative electrode, reducing the recombination of radiative electron-hole pairs and thus decreasing the PL intensity [14]. However, as research progresses, it has been found that the decrease in PL intensity observed on MAPbI<sub>3</sub> films used in solar cells is not universal. On the contrary, the addition of ionic liquids can passivate perovskite and inhibit ion migration. Especially with imidazole-related ionic liquids, they are likely to interact with the surface of perovskite, particularly at positively charged defect sites such as iodide vacancies [15]. The interaction between imidazole in the ionic liquid and the surface inhibits iodide ion migration, leading to changes in PL intensity. The two mechanisms leading to the decrease and increase in PL intensity of MAPbI<sub>3</sub> crystals treated with three ionic liquids under electric field are similar to this, as Figure 6 shows to explain the principles.

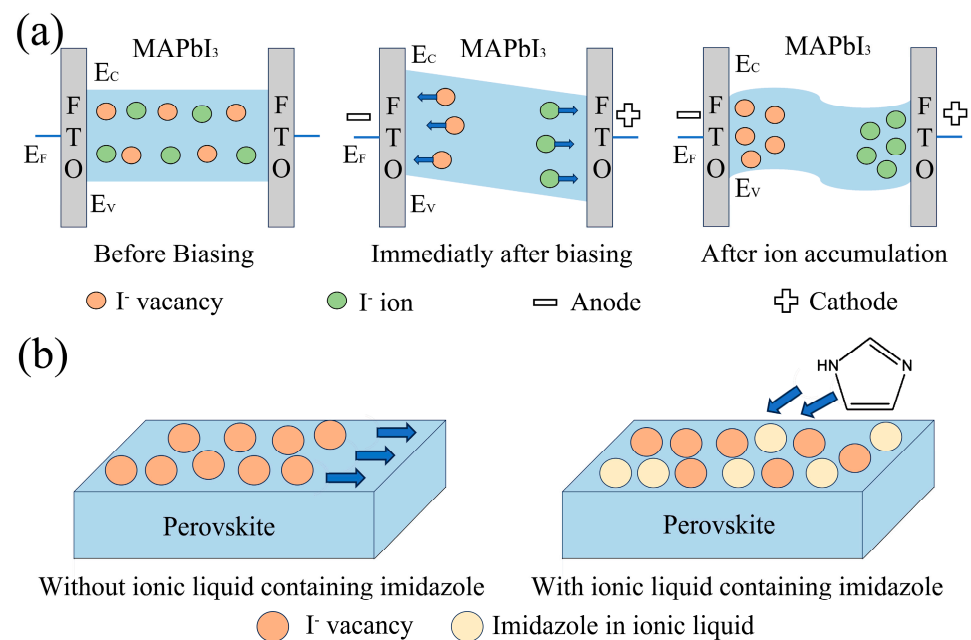


**Figure 6.** (a) Band diagrams at the different stages of ion migration and accumulation in early research; (b) Migration of iodine vacancies before and after the addition of imidazole-containing ionic liquid.

### 3.3. The Change Mechanisms of MAPbI<sub>3</sub> Crystal

To explore the electronic motion mechanism, the composition of MAPbI<sub>3</sub> crystals was analyzed using Escalab 250XI. The detection results are shown in Figure 7. The XPS spectral peak intensity represents the electron counts at specific binding energies, indicating the surface molar density magnitude of the elements. Comparing the X-ray photoelectron spectroscopy (XPS) of Pb elements in the crystals before and after immersion in ionic liquids, it is observed that the peak intensities representing the 4f<sub>5/2</sub> and 4f<sub>7/2</sub> orbitals both

decrease after immersion in ionic liquids. This means that the surface mole density of  $\text{Pb}^{2+}$  ions in all samples is less than the surface of untreated perovskite crystals. Interestingly, the characteristic peak representing the Pb simple substance all disappeared in the XPS spectrum of the three samples once electrified, while the three samples diluted with ETOH solution all surged. The opposite change in lead plasma peak position indicates that different mechanism changes occurred. In the electrification treatment method, the reduced lead ions undergo exciton recombination to reduce the defects, but the surface reduced lead ions precipitate in the ETOH dilution treatment.

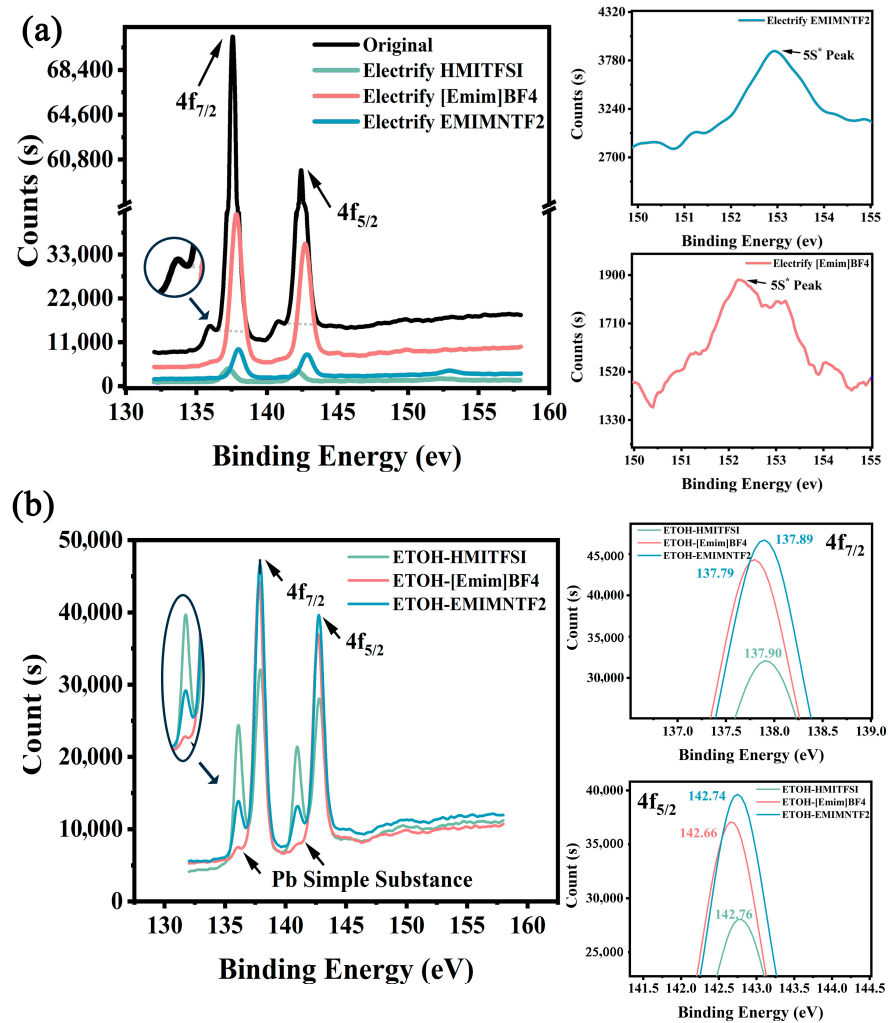


**Figure 7.** (a) XPS spectrum of Pb in  $\text{MAPbI}_3$  before and after electrically immersed in ionic liquid; (b) XPS spectrum of Pb in ETOH-ionic liquid  $\text{MAPbI}_3$ .

Meanwhile, in both Electrify-EMIMNTF2  $\text{MAPbI}_3$  and Electrify-[Emim]BF4  $\text{MAPbI}_3$ , peaks representing the  $5s^*$  orbitals are observed at around 153 eV. This indicates that both the electric immersion treatment with EMIMNTF2 and [Emim]BF4 cause the electrons of lead ions in  $\text{MAPbI}_3$  crystals to absorb energy during the ionization process of the ionic liquid, transitioning from the ground state of the  $4f_{5/2}$  and  $4f_{7/2}$  orbitals to the excited state of  $5s^*$ . Combining with the luminescent characteristics of  $\text{MAPbI}_3$  crystals, it can be inferred that during excitation, the transition that occurs is a  $\sigma-\sigma^*$  transition [16]. Such electron transitions are one of the reasons for the large increase in the peak intensity in PL spectra, where higher excitation photon energies and shorter wavelengths cause a large number of newly generated excitons to produce photoluminescence.

The characteristic peaks of the Pb simple substance are observed in the XPS spectra of all ETOH-ionic liquid MAPbI<sub>3</sub> three samples. A comparison of the two treatment methods reveals that the new system of ETOH-mixed ionic liquids lacks the important step of electrically driven immersion traditionally required by conventional ionic-liquid-treated materials. In the absence of voltage drive, ions in the new system are practically unable to pass through the grain boundary barrier and reach the interior of the grain boundary during the ETOH-mixed ionic liquid immersion of MAPbI<sub>3</sub> crystals. Therefore, unlike MAPbI<sub>3</sub> crystals treated with electrically driven ionic liquid immersion, those immersed in ETOH-ionic liquid do not undergo the same interactions within the crystal interior; the new system only improves the surface of MAPbI<sub>3</sub> [11].

### 3.4. The Characteristics of the X-ray Detector

To verify the effect of ionic liquid treatment on MAPbI<sub>3</sub> crystals in terms of X-ray detection, they were combined with rigid silicon-based electrodes to fabricate X-ray detectors. Figure 8a,b show the U-I characteristics of the detector while maintaining the X-ray power at 1200 W. On the other hand, Figure 8c,d depict the light power–current density curves obtained by fixing the voltage at 3V and varying the X-ray source voltage and current to change the X-ray power.

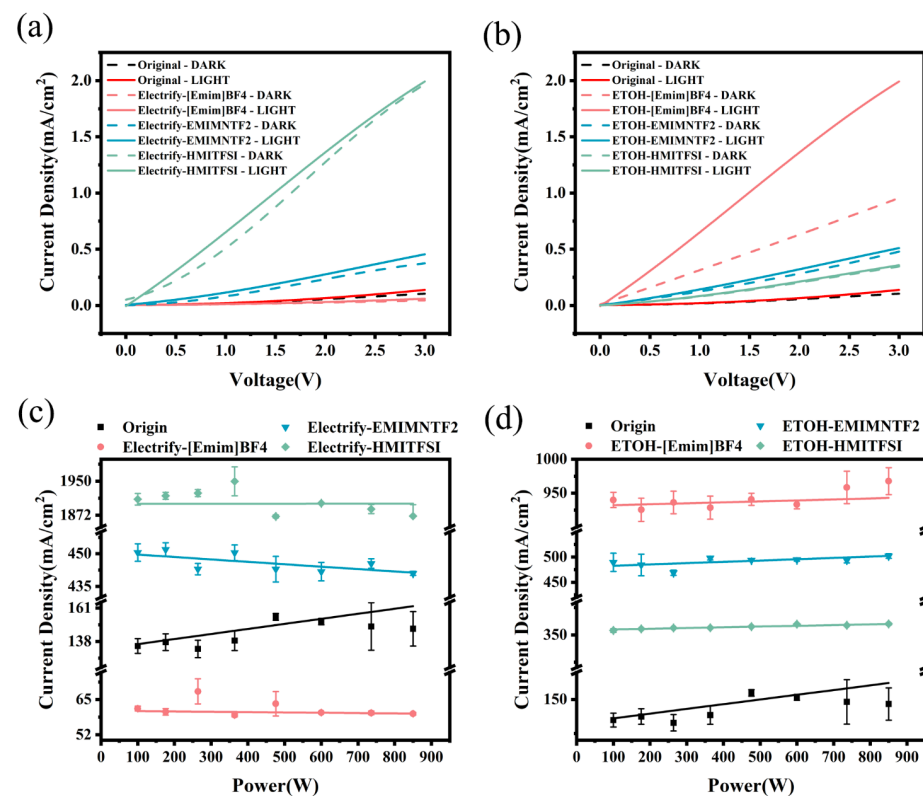


**Figure 8.** (a) Voltage–current density plot after ionic liquid electrification immersion; (b) voltage–current density plot after ionic liquid mixed ETOH immersion; (c) X-ray power and current density curves of MAPbI<sub>3</sub> before and after ionic liquid electrification immersion; (d) X-ray power and current density curves of MAPbI<sub>3</sub> before and after ionic liquid mixed ETOH immersion.

Compared with untreated MAPbI<sub>3</sub> crystals, Electrify-EMIMNTF2 MAPbI<sub>3</sub> and Electrify-HMITFSI MAPbI<sub>3</sub> exhibited a superior photoelectric current performance under the same X-ray excitation conditions. Specifically, the average photocurrent density of Electrify-EMIMNTF2 MAPbI<sub>3</sub> increased by 348.69% compared to untreated MAPbI<sub>3</sub>, while the average photocurrent density of Electrify-HMITFSI MAPbI<sub>3</sub> increased dramatically by 826.85%, far exceeding that of untreated MAPbI<sub>3</sub> in X-ray detection. This demonstrates

that the electrically driven immersion treatment of ionic liquids can effectively enhance the X-ray detection capability of MAPbI<sub>3</sub>. But the average photocurrent density of Electrify-[Emim]BF<sub>4</sub> MAPbI<sub>3</sub> decreased, indicating a decrease in photoelectric performance compared to before treatment. This suggests that different ionic liquids have varying effects on the performance of MAPbI<sub>3</sub> under the same treatment method.

However, unlike ionic liquid electrification immersion, the electrical properties of MAPbI<sub>3</sub> X-ray detectors were significantly enhanced after immersion treatment in ETOH-[Emim]BF<sub>4</sub> MAPbI<sub>3</sub> and ETOH-EMIMNTF2 MAPbI<sub>3</sub>. Under the same voltage, regardless of whether under illuminated or dark conditions, the current density of the X-ray detectors made from treated MAPbI<sub>3</sub> was higher than that of untreated ones. The improvement in electrical properties was evident. But the average photocurrent density of ETOH-HMITFSI MAPbI<sub>3</sub> decreased, indicating a decrease in photoelectric performance compared to before treatment.

To further investigate the performance changes in MAPbI<sub>3</sub> in X-ray detectors before and after treatment with ionic liquids, a fixed voltage of 3 V was used. By changing the voltage and current of the X-ray source, the power of the X-ray was altered to obtain the power–current density curves under illumination. The fitted linear K value represents the X-ray detector’s sensitivity [17]. It can be observed that the sensitivity of X-ray detectors made from Electrify-HMITFSI MAPbI<sub>3</sub> crystals is significantly increased by 72.6%. However, for X-ray detectors made from MAPbI<sub>3</sub> treated with ionic liquid electrification immersion, the sensitivity decreases compared to untreated MAPbI<sub>3</sub> X-ray detectors. Among them, the decrease is most pronounced for Electrify-[Emim]BF<sub>4</sub> MAPbI<sub>3</sub>, with a sensitivity even reaching 0.00123, indicating a responsiveness to X-rays of less than 2.32% of that of untreated MAPbI<sub>3</sub> X-ray detectors. Meanwhile, all three samples treated with ETOH-mixed ionic liquids showed a certain degree of decrease in sensitivity. Among them, the sample with the least decrease in sensitivity is ETOH-EMIMNTF2 MAPbI<sub>3</sub>, while the sensitivities of the other two samples decreased by 66.49% and 80.93%, respectively, compared to untreated MAPbI<sub>3</sub> X-ray detectors. The specific parameter values for all the X-ray detectors are listed in Table 1. The performances of the detectors are also compared with those of previous studies in Table 1. Compared with previous studies, the photocurrent density of the detectors is significantly improved.

**Table 1.** Photocurrent density and sensitivity of detectors.

Material	Treatment	Photocurrent Density	Sensitivity
MAPbI <sub>3</sub>	None	8.79 mA/cm <sup>2</sup>	0.05292 mA·w/cm <sup>2</sup>
MAPbI <sub>3</sub>	[Emim]BF <sub>4</sub> Electrify	4.677 mA/cm <sup>2</sup>	−0.00123 mA·w/cm <sup>2</sup>
MAPbI <sub>3</sub>	EMIMNTF2 Electrify	39.44 mA/cm <sup>2</sup>	−0.00472 mA·w/cm <sup>2</sup>
MAPbI <sub>3</sub>	HMITFSI Electrify	81.47 mA/cm <sup>2</sup>	−0.09134 mA·w/cm <sup>2</sup>
MAPbI <sub>3</sub>	ETOH mix [Emim]BF <sub>4</sub>	23.08 mA/cm <sup>2</sup>	0.01773 mA·w/cm <sup>2</sup>
MAPbI <sub>3</sub>	ETOH mix EMIMNTF2	23.40 mA/cm <sup>2</sup>	0.04702 mA·w/cm <sup>2</sup>
MAPbI <sub>3</sub>	ETOH mix HMITFSI	5.72 mA/cm <sup>2</sup>	0.01009 mA·w/cm <sup>2</sup>
MAPbI <sub>3</sub> [5]	None	7 μA/cm <sup>2</sup>	25 μC mGy <sub>air</sub> <sup>−1</sup> cm <sup>−3</sup>
MA <sub>3</sub> Bi <sub>2</sub> I <sub>9</sub> [18]	None	0.441 pA/pixel	1947 μC Gy <sub>air</sub> <sup>−1</sup> cm <sup>−2</sup>
MAPbBr <sub>3</sub> [19]	MAPbCl <sub>3</sub> pn heterojunction	0.63 nA/cm <sup>2</sup>	868 μC Gy <sub>air</sub> <sup>−1</sup> cm <sup>−2</sup>

Combined with the PL spectrum, it is interesting to find that perovskite crystal materials choose the same optimized ionic liquid species in X-ray detection and photovoltaic power generation applications, and the effect is quite the opposite. Particularly, Electrify-HMITFSI MAPbI<sub>3</sub> crystal exhibited a light intensity which decreased to about 90% of the original sample under 355 nm light emission. But the X-ray detector made from Electrify-HMITFSI MAPbI<sub>3</sub>, with a higher carrier recombination efficiency and easier separation of photogenerated electrons, demonstrated a superior X-ray and worse UV photovoltaic performance, as Figure 9 shows.

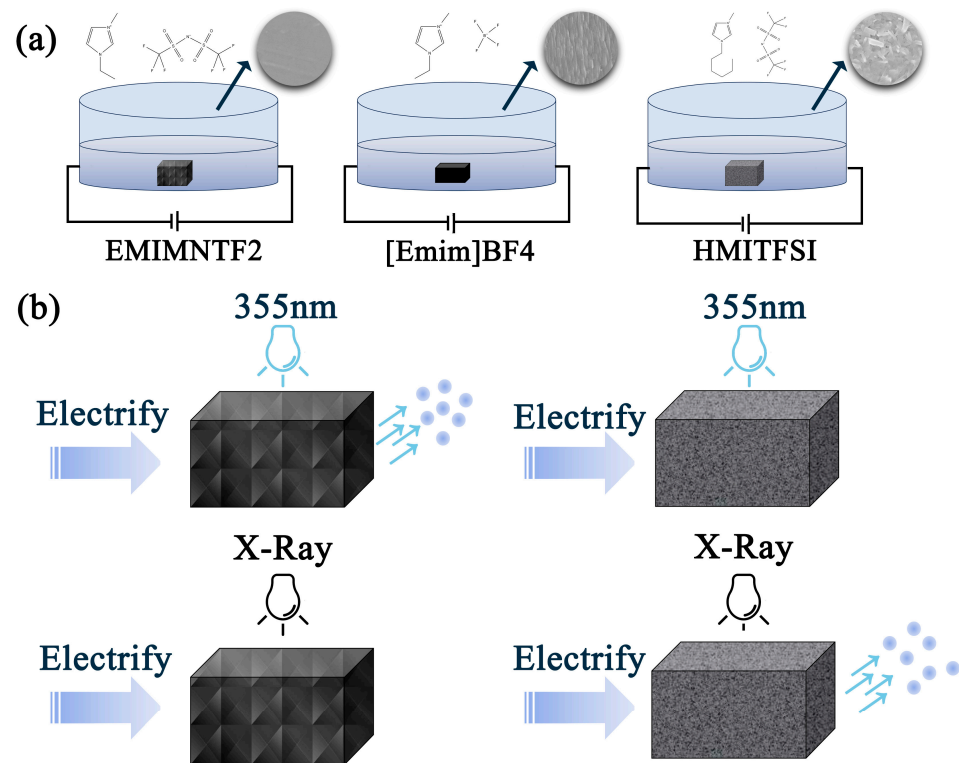


**Figure 9.** (a) Crystal treatment process, (b) different surface conditions create different photoelectric properties.

Combined with the previous results of the crystal performance, it can be inferred that the HMITFSI ionic liquid forms a squamous structure on the crystal surface, with the largest change in the crystal phase structure and the strongest dislocation boundary barrier. When the surface under 355 nm, the irradiation depth is limited and the number of electron  $\sigma\text{-}\sigma^*$  transition is limited, resulting in reduced PL intensity. However, in the voltage drive, ions are practically able to pass through the grain boundary barrier and reach the interior of the grain boundary in electrification treatment methods. All the composite excitons are trapped by the crystal boundary barrier and cannot be released; only when the X-rays shine. There is no limited depth of irradiation, the conversion of internal excitons to photogenerated charge carriers occurs to generate the maximum photocurrent. All the outer electrons are blocked by the crystal boundary barrier and cannot appear in the form of photocurrent; only when the x-ray irradiation, the high-energy photons convert the inner electrons into photogenerated carriers to be detected, and the grain boundary cannot be blocked, creating the maximum photocurrent. This mechanistic explanation also applies to the Electrify-EMIMNTF2 MAPbI<sub>3</sub> and Electrify-[Emim]BF<sub>4</sub> MAPbI<sub>3</sub> crystals material.

This trend is also evident in samples treated with ETOH-mixed ionic liquids. In contrast, MAPbI<sub>3</sub> treated with a mixture of ionic liquid and ETOH immersion lack the powerful ionization method of electrification immersion. The cations and anions cannot penetrate the grain boundaries of the MAPbI<sub>3</sub> but can only induce a certain degree of surface ionization through the interaction between ETOH and the ionic liquid, thereby improving the surface electron environment of the MAPbI<sub>3</sub>. Thus, ETOH-HMITFSI MAPbI<sub>3</sub>, which experienced the biggest decrease on average photocurrent density in three ETOH-ionic MAPbI<sub>3</sub>, is also the only sample in the PL spectrum that peak intensity decreased.

#### 4. Conclusions

In this study, we examined the influence of three ionic liquids—EMIMNTF<sub>2</sub>, HMITFSI, and [Emim]BF<sub>4</sub>—on the characteristics of MAPbI<sub>3</sub> for X-ray photodetectors. The findings indicate that these ionic liquids alter the properties of MAPbI<sub>3</sub> under two different

treatments. The surface morphology, crystal phase structure, photoluminescence, and electronic configuration of MAPbI<sub>3</sub> crystals by ionic liquid modification were characterized by SEM, XRD, PL, and XPS tests. The corresponding X-ray detector is made, and the photoelectric conversion characteristics and sensitivity of X-rays are tested. It is interesting to find that MAPbI<sub>3</sub> perovskite crystal materials choose the same optimized ionic liquid species in X-ray detection and photovoltaic power generation applications, and the effect is quite the opposite. The analysis shows that the type of ionic liquid determines the surface grain boundary barrier, ranging from EMIMNTF2, [Emim]BF<sub>4</sub>, to HMITFSI. The biggest difference between the two ionic liquid treatment methods is whether the ion can be passed through the crystal boundary barrier and delivered to the crystal interior. Compared with untreated MAPbI<sub>3</sub> crystals, the average photocurrent density of Electrify-HMITFSI MAPbI<sub>3</sub> increased by 826.85% under X-ray excitation and the sensitivity of X-ray detectors made from these treated MAPbI<sub>3</sub> crystals significantly increased by 72.6%, but the intensity of the PL spectrum decreased to 90% of the untreated intensity. The PL peak intensity of Electrify-EMIMNTF2 and ETOH-[Emim]BF<sub>4</sub> MAPbI<sub>3</sub> crystals increased by approximately 200% under UV light excitation, the average photocurrent density of X-ray detectors increased by 448% and 262%.

**Supplementary Materials:** The following supporting information can be downloaded at: <https://www.mdpi.com/article/10.3390/coatings14050633/s1>, Figure S1. (a,c) Preparation of MAPbI<sub>3</sub> SCs; (b,d) Completed MAPbI<sub>3</sub> SCs. Figure S2. The metal interdigital electrode with a size of 4 mm \* 6 mm. Figure S3. The structure of different phases MAPbI<sub>3</sub> crystals simulated by Material Studio (a) Cube (b) Tetragonal (c) Orthorhombic. Figure S4. The density of states of different phases MAPbI<sub>3</sub> SCs simulated by Material Studio (a) Cube (b) Tetragonal (c) Orthorhombic. Figure S5. The band structure of different phases MAPbI<sub>3</sub> SCs simulated by Material Studio (a) Cube (b) Tetragonal (c) Orthorhombic. Figure S6. XPS of ETOH-ionic liquid MAPbI<sub>3</sub> SCs (a) EMIMNTF2 (b) [Emim]BF<sub>4</sub> (c) HMITFSI. Figure S7. (a) XPS survey of electric immersion MAPbI<sub>3</sub> (b) I 3d scan of electric immersion MAPbI<sub>3</sub> (c) XPS survey of ETOH mixed immersion MAPbI<sub>3</sub> (d) I 3d scan of ETOH mixed immersion MAPbI<sub>3</sub>.

**Author Contributions:** X.S.: Conceptualization, writing—review and editing, equipment support, direction guidance, funding acquisition. R.W.: Conceptualization, investigation, validation, data curation, visualization, formal analysis, writing—original draft. H.Y.: Investigation, funding acquisition. J.W.: Equipment support, experimental assurance, funding acquisition. R.C.: Methodology. H.M.: Resources. L.W.: Supervision, project administration. All authors have read and agreed to the published version of the manuscript.

**Funding:** This work was supported by the National Natural Science Foundation of China under Youth Science Foundation Project (Grant Nos. 61805005 and 62305262). The International Research Cooperation Seed Fund of Beijing University of Technology (Grant Nos. 2021B34). Beijing University of Technology's "Introduction and Cultivation 2.0" Project (Grant Nos. 2024GW06).

**Institutional Review Board Statement:** Not applicable.

**Informed Consent Statement:** Not applicable.

**Data Availability Statement:** Data will be made available on request.

**Conflicts of Interest:** The authors declare that they have no known competing financial interests or personal relationships that could have appeared to influence the work reported in this paper.

## References

1. Borriello, I.; Cantele, G.; Ninno, D. Ab Initio Investigation of Hybrid Organic-Inorganic Perovskites Based on Tin Halides. *Phys. Rev. B* **2008**, *77*, 235214. [[CrossRef](#)]
2. Xiao, Z.; Song, Z.; Yan, Y. From Lead Halide Perovskites to Lead-Free Metal Halide Perovskites and Perovskite Derivatives. *Adv. Mater.* **2019**, *31*, e1803792. [[CrossRef](#)] [[PubMed](#)]
3. Mitzi, D.B. Templating and structural engineering in organic-inorganic perovskites. *J. Chem. Soc. Dalton Trans.* **2001**, *1*, 1–12. [[CrossRef](#)]
4. Dou, L.; You, J.; Hong, Z.; Chang, W.-H.; Li, G.; Yang, Y. Solution-processed hybrid perovskite photodetectors with high detectivity. *Nat. Commun.* **2014**, *5*, 5404. [[CrossRef](#)] [[PubMed](#)]

5. Yakunin, S.; Sytnyk, M.; Kriegner, D.; Shrestha, S.; Richter, M.; Matt, G.J.; Azimi, H.; Brabec, C.J.; Stangl, J.; Kovalenko, M.V.; et al. Detection of X-ray photons by solution-processed lead halide perovskites. *Nat. Photon.* **2015**, *9*, 444–449. [[CrossRef](#)]
6. Song, Y.; Li, L.; Bi, W.; Hao, M.; Kang, Y.; Wang, A.; Wang, Z.; Li, H.; Li, X.; Fang, Y.; et al. Atomistic Surface Passivation of  $\text{CH}_3\text{NH}_3\text{PbI}_3$  Perovskite Single Crystals for Highly Sensitive Coplanar-Structure X-Ray Detectors. *Applied Phys. Lett.* **2020**, *2020*, 5958243. [[CrossRef](#)]
7. Wang, F.; Duan, D.; Singh, M.; Sutter-Fella, C.M.; Lin, H.; Li, L.; Naumov, P.; Hu, H. Ionic Liquid Engineering in Perovskite Photovoltaics. *Energy Environ. Mater.* **2022**, *6*, e12435. [[CrossRef](#)]
8. Li, M.; Zhao, C.; Wang, Z.; Zhang, C.; Lee, H.K.H.; Pockett, A.; Barbé, J.; Tsoi, W.C.; Yang, Y.; Carnie, M.J.; et al. Interface Modification by Ionic Liquid: A Promising Candidate for Indoor Light Harvesting and Stability Improvement of Planar Perovskite Solar Cells. *Adv. Energy Mater.* **2018**, *8*, 1801509. [[CrossRef](#)]
9. Zhang, Z.; Guo, T.; Yuan, H.; Yu, L.; Zhao, R.; Deng, Z.; Zhang, J.; Liu, X.; Hu, Z.; Zhu, Y. Reconstruction of the  $(\text{EMIm})_x\text{MA}_{1-x}\text{Pb}(\text{BF}_4)_x\text{I}_{1-x}$  Interlayer for Efficient and Stable Perovskite Solar Cells. *ACS Appl. Mater. Interfaces* **2020**, *13*, 727–733. [[CrossRef](#)] [[PubMed](#)]
10. Zhao, L.; Wang, Z.; Dong, X. Effect of Ionic Liquid on the Performance of Perovskite Solar Cells. *Chin. J. Appl. Chem.* **2018**, *35*, 216–223.
11. Su, X.; Chen, R.; Pan, Y.; Wang, J.; Gao, D.; Yu, H.; Wang, Y.; Wang, L. High optical modulation efficiency in perovskite  $\text{CsPbI}_3/\text{Br}_3$  by ionic liquid ionization. *Opt. Mater.* **2023**, *136*, 113363. [[CrossRef](#)]
12. Xiao, J.; Liu, L.; Zhang, D.; De Marco, N.; Lee, J.; Lin, O.; Chen, Q.; Yang, Y. The Emergence of the Mixed Perovskites and Their Applications as Solar Cells. *Adv. Energy Mater.* **2017**, *7*, 1700491. [[CrossRef](#)]
13. Tian, G.; Wang, D.; Wang, P. Molecular Dynamics Simulations of Structure and Properties of 1-Ethyl-3-methylimidazolium Tetrafluoroborate Ionic Liquid and ETOH Mixture. *J. Kunming Univ. Sci. Technol.* **2012**, *37*, 21–27. (In Chinese) [[CrossRef](#)]
14. Deng, X.; Wen, X.; Lau, C.F.J.; Young, T.; Yun, J.; Green, M.A.; Huang, S.; Ho-Baillie, A.W.Y. Electric field induced reversible and irreversible photoluminescence responses in methylammonium lead iodide perovskite. *J. Mater. Chem. C* **2016**, *4*, 9060–9068. [[CrossRef](#)]
15. Shahiduzzaman, M.; Muslih, E.Y.; Hasan, A.M.; Wang, L.; Fukaya, S.; Nakano, M.; Karakawa, M.; Takahashi, K.; Akhtaruzzaman, M.; Nunzi, J.M.; et al. The benefits of ionic liquids for the fabrication of efficient and stable perovskite photovoltaics. *Chem. Eng. J.* **2021**, *411*, 128461. [[CrossRef](#)]
16. Zheng, Y.; Yao, Z.; Lei, T.; Dou, J.; Yang, C.; Zou, L.; Meng, X.; Ma, W.; Wang, J.; Pei, J. Unraveling the Solution-State Supramolecular Structures of Donor–Acceptor Polymers and their Influence on Solid-State Morphology and Charge-Transport Properties. *Adv. Mater.* **2017**, *29*, 1701072. [[CrossRef](#)]
17. Song, Y. *Research of Perovskite Single Crystal Photoelectric Devices with Precision Control of Surface States*; Jilin University: Changchun, China, 2021. (In Chinese) [[CrossRef](#)]
18. Liu, Y.; Xu, Z.; Yang, Z.; Zhang, Y.; Cui, J.; He, Y.; Ye, H.; Zhao, K.; Su, H.; Lu, R.; et al. Inch-Size 0D-Structured Lead-Free Perovskite Single Crystals for Highly Sensitive Stable X-Ray Imaging. *Matter* **2020**, *3*, 180–196. [[CrossRef](#)]
19. Yan, J.; Gao, F.; Tian, Y.; Li, Y.; Gong, W.; Wang, S.; Zhu, H.; Li, L. Controllable Perovskite Single Crystal Heterojunction for Stable Self-Powered Photo-Imaging and X-Ray Detection. *Adv. Opt. Mater.* **2022**, *10*, 2200449. [[CrossRef](#)]

**Disclaimer/Publisher’s Note:** The statements, opinions and data contained in all publications are solely those of the individual author(s) and contributor(s) and not of MDPI and/or the editor(s). MDPI and/or the editor(s) disclaim responsibility for any injury to people or property resulting from any ideas, methods, instructions or products referred to in the content.